CORA Cork Open Research Archive
Cartlann Taighde Oscailte Chorcaí

Title	Numerical hydrodynamic modelling of a pitching wave energy converter
Authors	Bhinder, Majid A.;Rahmati, M. T.;Mingham, C. G.;Aggidis, G. A.
Publication date	2015-11-13
Original Citation	Bhinder, Majid A.; Rahmati, M. T.; Mingham, C. G.; Aggidis, G. A. (2015) 'Numerical hydrodynamic modelling of a pitching wave energy converter'. European Journal Of Computational Mechanics, 24 (4):129-143. doi: 10.1080/17797179.2015.1096228
Type of publication	Article (peer-reviewed)
Link to publisher's version	https://www.tandfonline.com/doi/full/10.1080/17797179.2015.1096228 - 10.1080/17797179.2015.1096228
Rights	© 2015 Informa UK Limited. This is an Accepted Manuscript of an article published by Taylor & Francis in European Journal of Computational Mechanics on 13 Nov 2015, available online: http://www.tandfonline.com/10.1080/17797179.2015.1096228
Download date	2026-11-07 21:00:40
Item downloaded from	https://hdl.handle.net/10468/7912



UCC
University College Cork, Ireland
Coláiste na hOllscoile Corcaigh

Numerical Hydrodynamic Modelling of a Pitching Wave Energy Converter

Majid A. Bhinder[a,*], M. T. Rahmati[b,*], C.G. Mingham[c], G.A. Aggidis[d]

[a]*Marine Renewable Energy Ireland (MaREI),*
University College Cork,
Cork, Ireland.
[b]*Mechanical, Aerospace and Civil Engineering Department,*
Brunel University,
Uxbrdige, UB8 3PH, UK.
[c]*Department of Computing and Mathematics,*
Manchester Metropolitan University,
M1 5GD Manchester, UK.
[d]*Renewable Energy Group,*
Faculty of Science and Technology,
Lancaster University, LA1 4YR Lancaster, UK.

Abstract

Two computational methodologies – CFD (*computational fluid dynamics*) and the numerical modelling using linear potential theory based *boundary element method* (BEM) are compared against experimental measurements of the motion response of a pitching wave energy converter. CFD is considered as relatively rigorous approach offering nonlinear incorporation of viscous and vortex phenomenon and capturing of the flow turbulence to some extent, whereas numerical approach of the BEM relies upon the linear frequency domain hydrodynamic calculations that can be further used for the time domain analysis offering robust preliminary design analysis. This paper reports results from both approaches and concludes upon the comparison of numerical and experimental findings.

Keywords: WEC, numerical modelling, CFD, FLOW-3D, hydrodynamic, pitching, wave energy converter, AQWA.

*Corresponding author
Email addresses: mbhinder@ucc.ie (Majid A. Bhinder), mt.rahmati@gmail.com (M. T. Rahmati)

1. Introduction

Point absorber wave energy concept named WRASPA (Wave-driven, Resonant, Arcuate action, Surging Point-Absorber) is a pitching surge mode motion *wave energy converter* (WEC) which had been developed at Lancaster University and was designed to be deployed at water depths of 20-50 meter. In this device, wave forces act on the face of a collector body carried on an arm that rotates about a fixed horizontal axis below sea level. Accordingly, the body oscillates at about the frequency of the ocean swell generating high power from a small device. In storms the arm below sea level automatically moves to a position that minimises forces and so ensures its survival. A diagram showing the collector body which rotates around a specified pivot is shown in Figure 1 whereas artists' impression of the device dynamics and free surface level is presented in Figure 2.

The experimental and numerical results show that pitching-surge point absorber WECs have the potential to generate high power from relatively small devices (Chaplin and Folley, 1998; Chaplin and Aggidis, 2007; Rahmati et al., 2008a).

Numerical study of a WEC has a potentially great impact on possible design changes at an early stage in the model design. Several design configurations can be tested numerically at a much lower cost compared to an experimental setup. Major issues, however, related to numerical modelling of such devices include proper handling of the free surface interface, wave-structure interaction and wave reflection at wall boundaries.

For computational hydrodynamic analysis of point absorber wave energy converter two approaches are usually employed. One is based on the linear potential theory approach and the second is the *Reynolds Averaged Navier Stokes Equations*(RANSE) based CFD methodology.

Linear theory is a reasonably good choice when modelling floating structures to replicate small scale laboratory tests but is bound to miscarry in extreme situations (Thomas, 2008).

De Backer et al. (2009) showed results from linear theory computations against experimental tests. Frequency and time domain equations for a generic heaving buoy are considered. Good accuracy is reported for regular waves whereas in the instance of irregular waves the predicted power tends to differ from experimental values by less than 20%. It was reported that the results of the resonance situation (that is where the incoming wave frequency approaches the natural frequency of the device) are not in favourable agreement with experimental findings. This implies, when device oscillates with a much higher amplitude (being in resonance

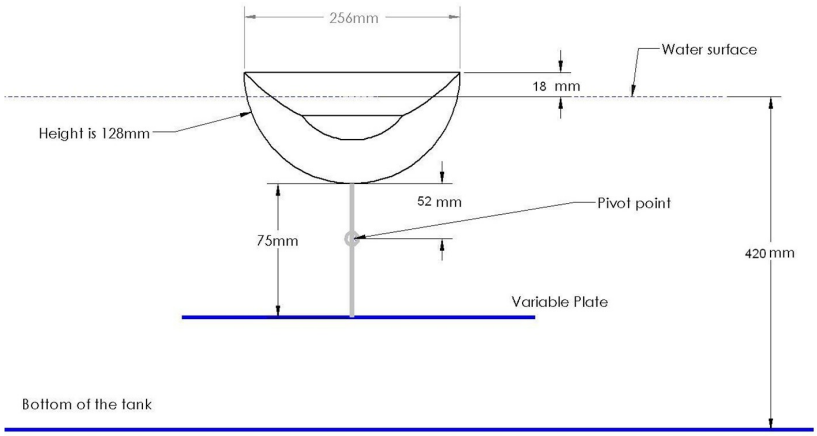


Figure 1: Schematic of the WEC

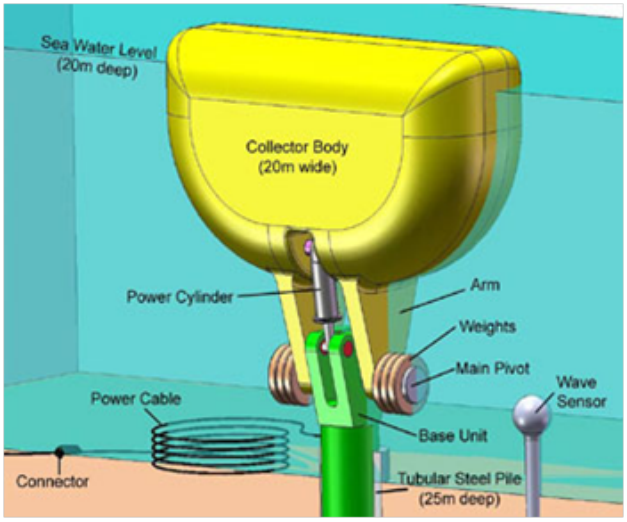


Figure 2: Artist impression of the WEC

situation), the small motion assumption of linear theory becomes invalid.

Babarit et al. (2009) presented two different approaches in order to overcome the limitations of the linear theory to model a floating wave energy converter. The first one offers hydrostatic and Froude-Krylov forces to be computed at the exact instantaneous positions of the moving body (a similar methodology to Gilloteaux et al. (2007)). In the second approach the solver based on modified *Reynolds-*

averaged NavierStokes Equations (RANSE) is used. The comparisons of both approaches with experimental data showed good agreement. However it was observed that the computing time of the latter was considerably longer than the former. It was shown that potential flow description of wave representation does have the advantages of smooth propagation together with ease of computational time.

Recently, in Li and Yu (2012) a review of analytical and numerical methods for point absorber type wave energy conversion systems is reported in detail and *boundary element method* also referred as *Boundary integral equation method* (BIEM) is explained alongside CFD or *NavierStokes equation methods* (NSEM). Moreover an empirical drag term of the Morison equation is discussed in relation to the viscous drag.

In Bhinder et al. (2012), CFD is employed to quantify the drag damping coefficient for surging floating device and this drag coefficient is then added into the time domain model which rely upon the frequency domain results of the BEM methodology. Using CFD and BEM methodology (Bhinder et al., 2015) showed that drag losses greatly influence the output power production of a surging wave energy converter.

Causon et al. (2008); Hu et al. (2009) reported cartesian cut cell based RANSE solver for the CFD modelling of generic wave energy device . In (Hu et al., 2009) total simulation time was not mentioned however the reported CPU time of 11 days highlights computing time issue. This being one of the major issues associated with the CFD modelling of wave energy devices is under continuous development.

Thilleul et al. (2011) presented a numerical study of a wave energy converter using three computational methodologies: potential theory code, RANSE, and a *smoothed particle hydrodynamics* (SPH) solver. Results conclude that the potential flow solver offers relatively quick parametric analysis within reasonable range of accuracy when compared to the RANSE solver. And the difference between the former and lateral is reported to reach 20% when the linear assumptions are no longer valid.

In this paper, for a small scale floating device, BEM results are shown against CFD and experimental findings and this highlights the role of viscous and vortex forces for the resulting motion of a small scale device. This work focuses on the results of an experiment of WRASPA acting in pitch motion mode only and numerical study of two computational methodologies – CFD and potential flow theory based BEM method – is then discussed against experimental measurements. CFD computations are performed using commercial CFD code FLOW-3D while BEM based numerical modelling is achieved through commercial hydro-

dynamic package ANSYS AQWA. Setup of computational simulation for regular monochromatic waves is explained. Experimental data is taken from the small scale laboratory tests of the 1:100 scale model of the point absorber wave energy converter which is hinged at a point below the water surface and is allowed to move in pitch motion around y axis. The work is aimed at simulating a surging wave energy converter to achieve an optimized shape and to predict output power at a higher or full scale.

2. Experiment setup

The development and small scale wave tank tests of WRASPA have been performed by Rahmati et al. (2008a,b) at Lancaster University. The Length, width and height of the tank is 12m, 2.5m and .85m respectively. A snap of the experimental setup is shown in Figure 3.

This point absorber wave energy converter is relatively small compared to the most common sea wavelengths, and has the potential for more efficient power conversion, in terms of output per unit volume. However, smaller devices tend to have natural frequency responses of narrow bandwidth, only achieving high efficiency when excited by waves with a frequency around their resonance point. Optimum power output is obtained when the motion of the device is controlled so that the phase and amplitude of oscillation have specific optimum values, known as tuning the device. A stepwise control system has also been devised for extracting optimum power from irregular waves (Aggidis et al., 2009). The experimental study of both free and controlled motion of the device, in linear and non-linear waves, has led to an improved understanding of WRASPAs interaction with incoming waves. This has also provided valuable test data for evaluation various computational modelling capabilities.

An interesting decay test has been carried out to measure WRASPAs natural frequency. In the decay test the device is pulled in still water toward maximum displacement and then released while recording the time history of its position. The experimental study revealed that changing the freeboard or pivot depth controls the natural frequency of the device. Thus, this serves as an easy way of tuning the device according to the desired frequency spectrum. This experimental data is used in this study to evaluate the capabilities of two numerical modelling.

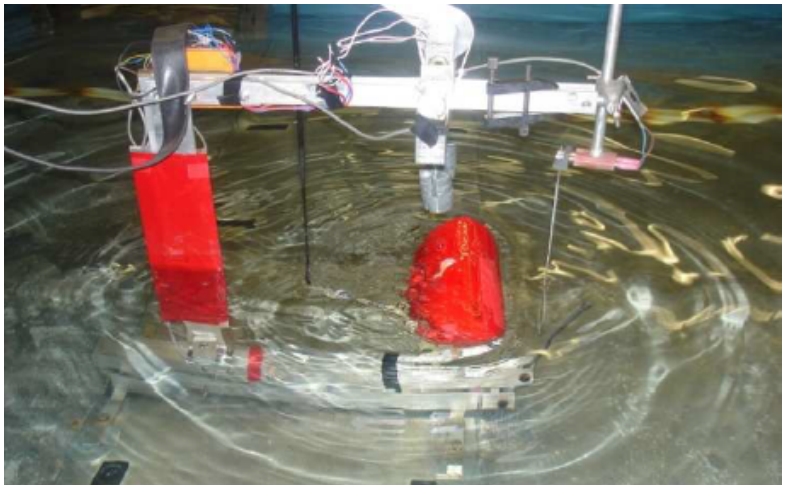


Figure 3: 1:100 scale model of the device in experimental wave tank

3. CFD setup

CFD analysis presented here was first reported in (Bhinder et al., 2009) where it was shown, for the first time, that such wave energy converter can be modelling using FLOW-3D. However for completeness CFD methodology is mentioned here in detail. FLOW-3Ds one fluid model (single fluid with free surface) was used to test wave propagation. It was observed that the decay in the wave amplitude (as it propagates) is much less and the solver was found to be relatively efficient in terms of computing time. A 3D simulation of a wave in a tank of dimensions 35m x 2.5m x 1.5m took about 5 hours using 793638 cells. FLOW-3D uses a structured mesh for its computational domain. Use of a single fluid with a free surface is based on the idea of volume fraction (F). Thus F=1 in the fluid region and F=0 in the other part of the domain (named the void region). Void regions have uniform pressure assigned and there is no fluid mass in these regions. This model does not require extra cells at the free surface hence reducing both setup and simulations run time. The ability to modify the mesh and geometry shape independently was another help in reducing simulation setup time.

The motion of the WRASPA device was modelled using the General Moving Object (GMO) model of FLOW-3D. The GMO model offers a fixed mesh method to simulate moving objects within the computational domain. The model was found to be robust and accurate. For all simulations, the shared memory parallel (SMP) version of FLOW-3D (v 9.3.1) was used. This version uses all available processors on the same machine which can also be regarded as locally parallel.

3.1. Meshing

In FLOW-3D the technique that defines the geometry of the solid structures is named as $FAVOR^{TM}$. This technique is based on the concept of area fraction (AF) and volume fraction (VF) of the rectangular structured mesh. Thus the geometry shape depends on the mesh cells that lie on the boundary of the structure. As the shape of the rigid body depends on the area and volume fractions of occupied cells, a local fine mesh was needed to establish the exact geometric shape of the rigid body. An optimum mesh was obtained by adding extra fixed points in the vicinity of the WEC. The way how this mesh renders the geometrical shape of the rigid body is further explained with the help of an illustration; see Figure 4, where the geometrical shape corresponding to three different mesh cell sizes is shown and it can been seen that to obtain a desired geometry shape, with higher precision, a much refined cell size would be required. In the present simulations, the sharp edges of the wave energy converter are to play a very important role in generating vortices, which in turn would influence the total viscous drag force. Therefore a fixed point method of the FLOW-3D-mesh generation was used and a smaller cell size at the fixed point insured that flow field in this region of oscillating motion would be resolved, this insured that the shape of the body edges will not be lost as the structure oscillates.

An optimum mesh profile can efficiently play an important role in minimizing the reflection effect caused at the outer domain boundaries therefore a stretched cells structure was achieved adjacent to these far-end boundaries as is shown in Figure 5.

3.2. Boundary conditions

Boundary conditions applied to the CFD wave are explained in Table 1 where the face numbers correspond to the Figure 6. To minimize wave reflection from the downstream (right hand side) end of the wave tank, the outflow boundary condition was applied together with stretched cells adjacent to this boundary. Initial condition of hydrostatic pressure along the depth of the wave tank was implemented.

3.3. Turbulence model

The RNG model was employed throughout all simulations unless stated otherwise. This model is based on the *Renormalization Group* (RNG) methods. In this approach the derivation of the turbulence quantities such as turbulent kinetic energy and the corresponding dissipation rate is accomplished using statistical methods.

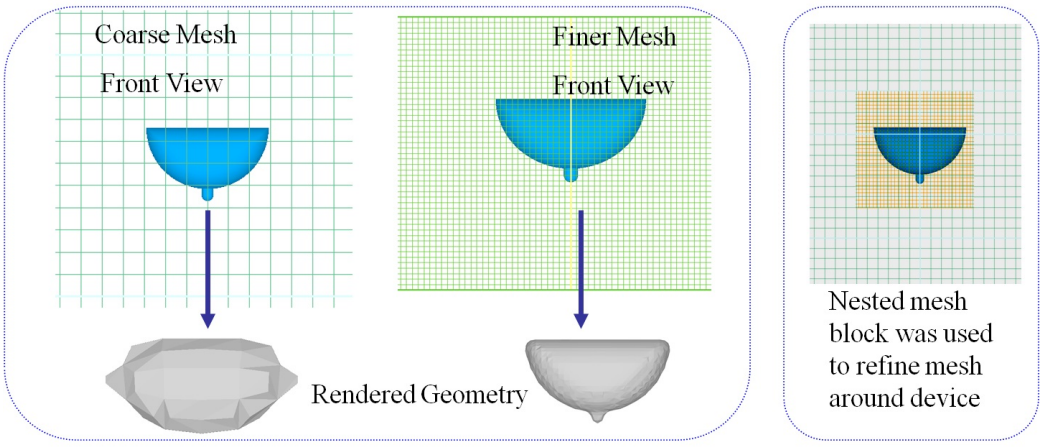


Figure 4: Mesh blocks and resulting shape of the rigid body

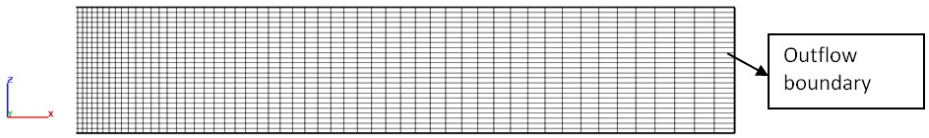


Figure 5: Stretched bigger cells at right boundary

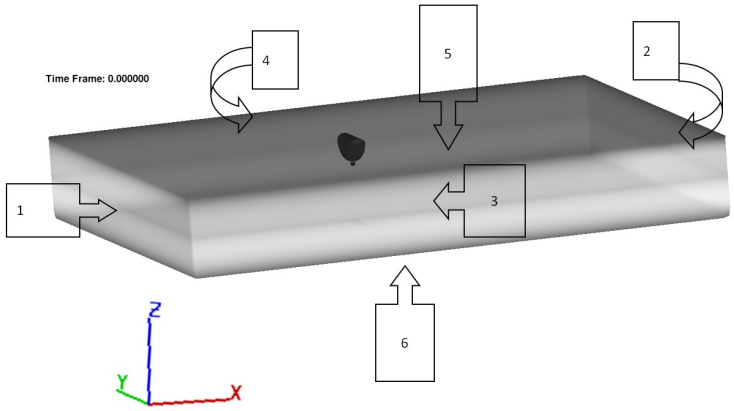


Figure 6: Boundary condition for CFD wave tank

Table 1: Boundary conditions explained

Face Number	Face of NWT	Boundary condition
1	Left - X min	Wave boundary
2	Right -X max	Outflow
3	Front -Y min	Symmetry
4	Back -Y max	Symmetry
5	Top - Z max	Fixed pressure
6	Bottom -Z min	Wall

The RNG model is based on the similar equations as the $k-\varepsilon$ model but the constants of these equations are found explicitly whereas in $k-\varepsilon$ model these coefficients are obtained empirically. RNG model is known to describe strong shear regions of the flow more accurately. The minimum value of the rate of the turbulent energy dissipation ε_T is limited according to the following equation

$$\varepsilon_{T,min} = C_\nu \sqrt{\frac{3}{2}} \frac{{k_T}^{3/2}}{T_{LEN}} , \tag{1}$$

where C_ν is a parameter (0.09 by default), k_T is the turbulent kinetic energy and T_{LEN} is the turbulent length scale. A constant value for this length scale is chosen according to the rule of 7% of the dominating moving body's dimension. Further details on the turbulent models and corresponding equations models is available in (FLOW-3D, 2009).

3.4. Equations of motion for a moving body in FLOW-3D

A rigid body motion is considered as a combination of translational and rotational motion. The velocity of any point on a moving body is equal to the velocity of the arbitrary base point plus the velocity due to the rotation of the object about that arbitrary point. For 6 degree-of-freedom motion, the GMO model considers the mass center G of the moving body as the base point. The equations of motion governing two separate motions (translational and rotational) for 6 degree-of-freedom motion are

$$\vec{F} = m\frac{d\vec{V_G}}{dt} , \tag{2}$$

$$\vec{T_G} = [J].\frac{d\vec{\omega}}{dt} + \vec{\omega} \times ([J].\vec{\omega}) , \tag{3}$$

where F is the total force, m is rigid body's mass, T_G is the total torque about G and $[J]$ is moment of inertia tensor about G in a body fitted reference system. The total force and total torque are calculated as the sum of several components as

$$\vec{F} = \vec{F_g} + \vec{F_h} + \vec{F_c} + \vec{F_{ni}} \tag{4}$$

$$\vec{T} = \vec{T_g} + \vec{T_h} + \vec{T_c} + \vec{T_{ni}} \tag{5}$$

where $\vec{F_g}$ is gravitational force, $\vec{F_h}$ is hydrodynamic force due to the pressure field and wall shear forces on the moving structure, $\vec{F_c}$ is the net control force prescribed to control or restrict the body's motion and $\vec{F_{ni}}$ is the non-inertial force if a rigid body moves in a non-inertial space system. In our case, $\vec{F_{ni}}$ is not present. Similarly, $\vec{T_G}$,$\vec{T_g}$,$\vec{T_h}$,$\vec{T_c}$ and $\vec{T_{ni}}$ are the total torque, gravitational torque, hydraulic torque, control torque and non-inertial torque about the mass center respectively.

Further detail about underlying mathematical model and numerical scheme is available in (FLOW-3D, 2009).

4. Numerical modelling in BEM

ANSYS AQWA was used to compute linear hydrodynamic coefficients such as added mass, radiation damping and the wave excitation force coefficients using 3 dimensional radiation/diffraction theory. In this potential theory, the incident wave field is assumed to be composed of harmonic wave and is relatively of small amplitude compared to its wavelength. The fluid is considered as ideal, incompressible, and irrotational. Based on the frequency response hydrodynamic coefficient the time domain motion response of the body is computed. For further detail of the underlying methodology see (ANSYS, 2014).

Surface mesh used in ANSYS AQWA computations is composed of quad and triangular surface panels as is shown in Figure 7. Mesh convergence was investigated using three different meshes.

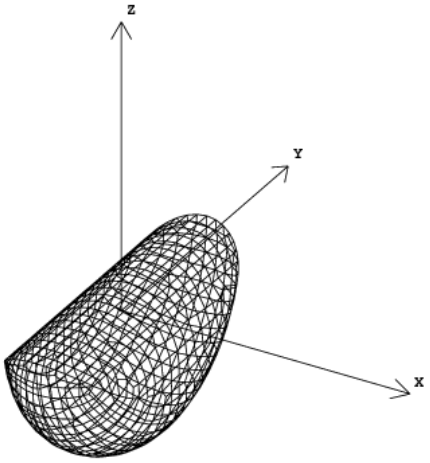


Figure 7: Surface panel mesh in ANSYS AQWA

5. Results and discussion

5.1. Mesh convergence test

In these tests three different mesh sizes (for block 1) were used for the same simulation and the results of each test were compared (see Figure 8) along with CPU time. In each test the mesh size of block 2 was kept constant. Table 2 shows the total number of cells, the smallest cell size (in the whole tank) and the time taken for each case. It can be seen in Figure 8 that the 3 meshes gave practically the same results. Therefore Mesh-1 was used for subsequent simulations to speed up compute time.

Table 2: Simulations for mesh indepence test

Mesh	Total cells	Smalles cell size [m]	CPU time for 13 sec wall time
Mesh-1	991188	0.01	1 day 8 hr
Mesh-2	1252904	0.008	1 day 14 hr
Mesh-3	1968372	0.006	3 days

5.2. Comparison of numerical modelling and experiments

5.2.1. Decay test

This test was used to measure the natural frequency of the device. For this purpose the device, from its resting vertical location in still water, was pulled

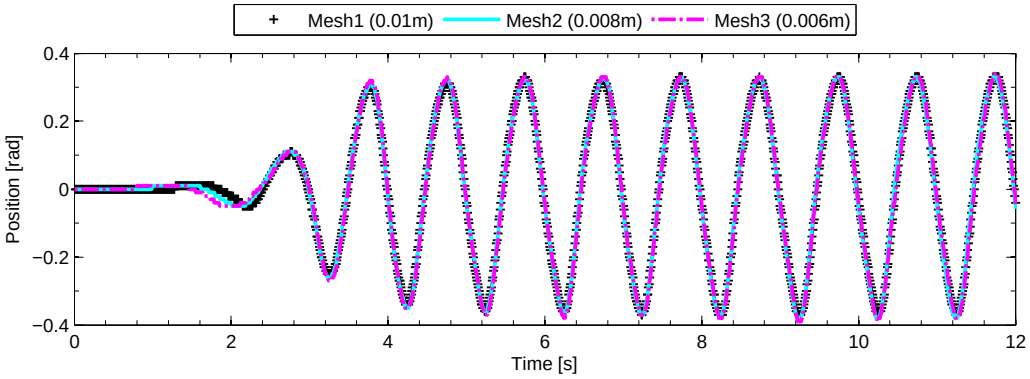


Figure 8: Comparison of device position for three different mesh profiles

towards one end and held for a few seconds so that the disturbed free surface became calm. Then the device was released and its damped oscillatory motion was measured. Numerical modelling of this test was conducted in two separate stages (see Figures 9 - 10). Firstly, the device was moved to 0.4 rad from the vertical by assigning a constant velocity on the walls of the collector body for 3 seconds and was held at 0.4 rad for another 1 second to allow time for the water surface to return to its initial calm state. Secondly, starting from the result file of the first stage, the device was released.

From the experimental results it was found that the natural frequency of the device was a function of freeboard and pivot depth. This natural frequency should equal the incoming waves frequency to get maximum power output. From the decay test the optimum value of the freeboard and pivot depth was found (to tune the natural frequency of the device to 1Hz approx). A comparison of numerical and experimental results for the decay test is given in Figure 11.

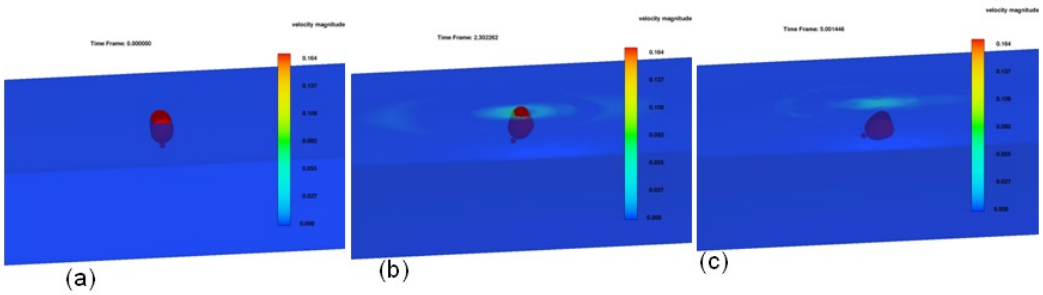


Figure 9: First stage of the decay test: (a) initial position, (b) medium deflection (c) maximum deflection

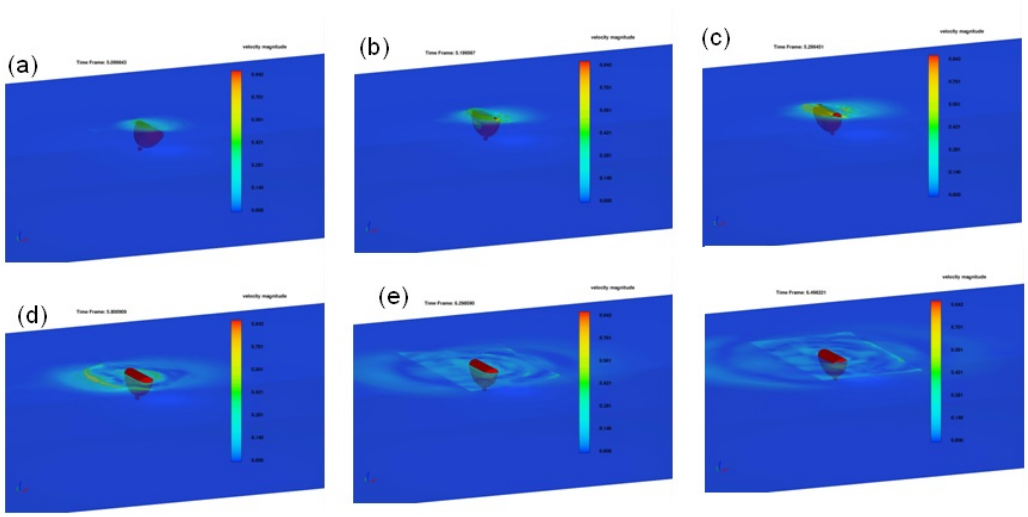


Figure 10: Second stage of the decay test at t seconds (a) t=0 (b) t=5.20 (c) t=5.30 (d) 5.80 (e) t=6.30 (f) t=6.50

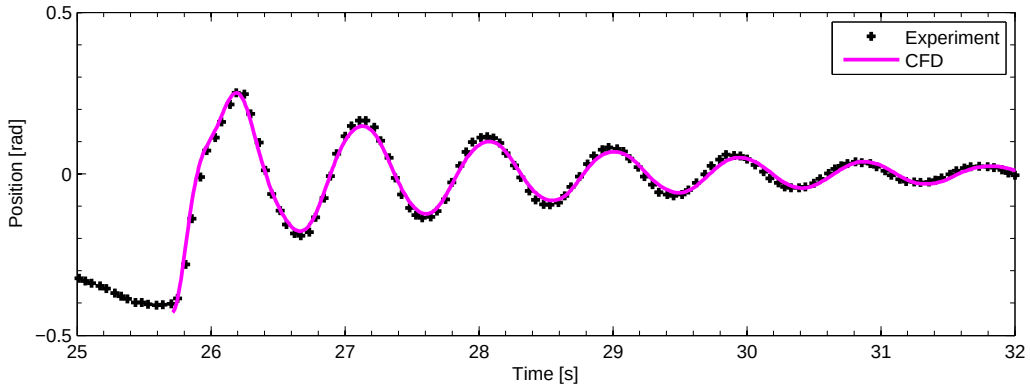


Figure 11: Results from the decay test, experiment and CFD

5.2.2. Free pitch motion

A comparison of CFD and experimentally measured results is shown in Figure 12 where angular displacement of the mass center of the device for an incident harmonic wave with amplitude 10mm and frequency 1Hz is shown. Recent computations from BEM solver are shown against CFD. Here it is evident that BEM solver offer slight overestimation when compared to CFD.

Analyzing these resulting comparison plot one can conclude that CFD results owing to numerical viscosity are in reasonable agreement with the laboratory measurements of (Bhinder et al., 2009). A comparison of CFD and BEM solution presented in Figure 12 shows that since viscous force term is not used in the time domain model and as the surface breaking is also omitted in BEM therefore observed differences between CFD and BEM could possibly be justified. However it is shown that for a small wave; BEM solution is within reasonable agreement with the experimental measurements. One possible reason of the small discrepancy of CFD results that can be seen at the negative side of the displaced position, could be the unnecessary damping caused by the numerical viscosity in the CFD computations, second differences in incident wave profile may have played a role. Along positive motion, it is observed that the CFD results show better agreement with the experiments whereas BEM computation show amplified response.

It is noticed that the computation cost of the BEM solver is much less than the CFD analysis. For a computation of hydrodynamic coefficients for a set of 20 frequencies, BEM solver took about 2 minutes of the wall clock time and the corresponding time domain response of the device for a single wave took

about 6 minutes of wall clock time for a simulation of 50 seconds. Whereas CFD computing time, as shown in Table 2, for a single wave of 13 seconds simulation is reported to be around 1 day and 8 hours to a maximum of 3 days depending on the mesh size.

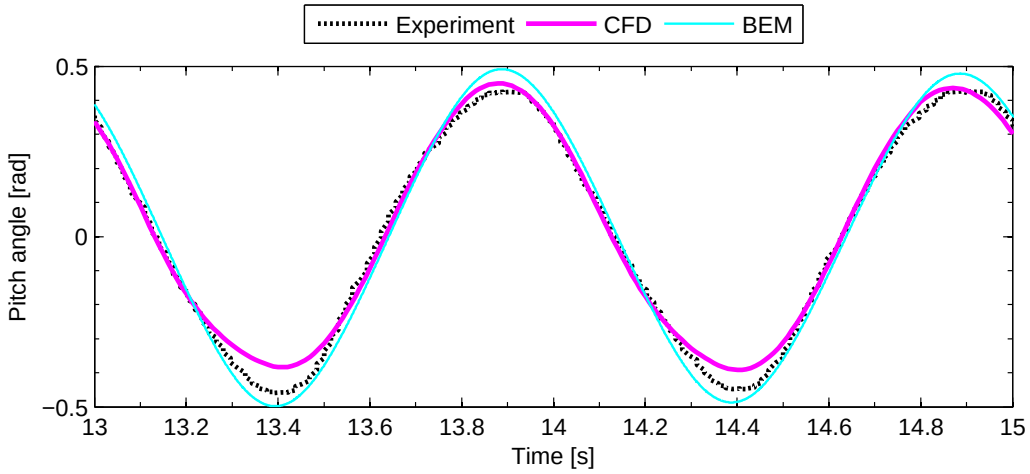


Figure 12: Free motion test for 10mm wave, experiment, CFD and BEM

For visual comparison with experimental setup shown in Figure 3; CFD contour plot is presented in Figure 13 where instants of device rotation and radiated wave field can be observed.

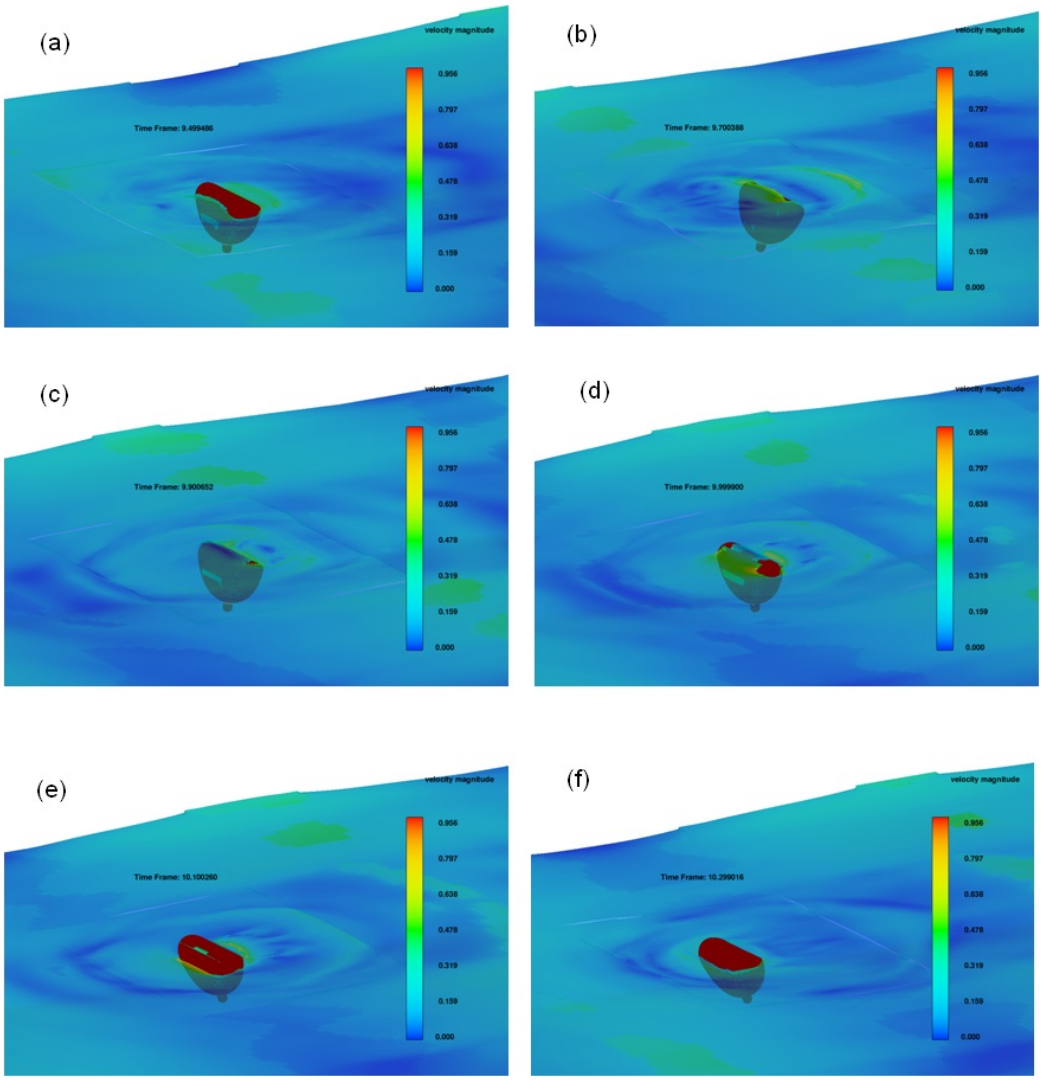


Figure 13: Instants of wave interaction of WEC from CFD computation

6. Conclusions

Two numerical methodologies, a high fidelity computational fluid dynamics method and a low fidelity boundary element method (BEM) are used for modelling the motion response of a pitching wave energy converter. The capabilities of the methods are validated against corresponding experimental data. It is recognized that flow models and solution methods of different fidelities and thus different expenses are needed for a range of design and troubleshooting problems. Time domain CFD methods offer in-corporation of viscous and vortex phenomenon and capturing flow details such as turbulence. These methods however, require significant computer resources and long run-times. The BEM method on the other hand, relies on the linear frequency domain hydrodynamic calculation which provides an efficient numerical approach capable of capturing the major features of interest while reducing the solution time to an acceptable level for use in routine design. This paper demonstrates the capability of the BEM method in capturing the flow information and the great advantage of significant CPU time saving.

7. Acknowledgment

Authors like to acknowledge that the CFD and the experimental work presented here was funded by Joule Centre, UK, Grant No: JIRP306/02 and authors are thankful to D.M.Causon and R.V.Chaplin for their invaluable support. Recent work using ANSYS AQWA is conducted at MaREI, UCC while the author was supported by the Science Foundation Ireland (SFI) under the Charles Parsons Award.

References

Aggidis, G. A., Rahmati, M., Chaplin, R., McCabe, A. P., Mingham, C., Causon, D., Bhinder, M., 2009. A control system for a new wave energy converter in irregular wave climates. In: 28th ASME International Conference on Ocean, Offshore and Arctic Engineering.

ANSYS, 2014. Aqwa theory manual v. 14.5. ANSYS Inc.

Babarit, A., Mouslim, H., Clément, A., Laporte-Weywada, P., 2009. On the numerical modelling of the non linear behaviour of a wave energy converter. In: 28th International Conference on Ocean, Offshore and Arctic Engineering (OMAE). ASME.

Bhinder, M. A., Babarit, A., Gentaz, L., Ferrant, P., June 2012. Effect of viscous forces on the performance of a surging wave energy converter. In: Twenty-second International Offshore and Polar Engineering Conference ISOPE. Rhodes, Greece.

Bhinder, M. A., Babarit, A., Gentaz, L., Ferrant, P., 2015. Potential time domain model with viscous correction and CFD analysis of a generic surging floating wave energy converter. International Journal of Marine Energy 10, 70 – 96.

Bhinder, M. A., Mingham, C. G., Causon, D. M., Rahmati, M. T., Aggidis, G. A., Chaplin, R. V., 2009. Numerical modelling of a surging point absorber wave energy converter. In: 8th European Wave and Tidal Energy Conference EWTEC. Uppsala, Sweden.

Causon, D., Qian, L., Hu, Z., Mingham, C., 2008. Cfd modeling of wave loads on offshore wave energy devices. Proceedings of the 18th ISOPE, 137–142.

Chaplin, R., Folley, M., 1998. Sea-bed devices technical comparisons of existing and new types. In: 4^{th} European Wave Energy Conference, Patras.

Chaplin, R. V., Aggidis, G. A., 2007. Wraspa: Wave interactions and control for pitching-surge point-absorber wave energy converters. In: Proceedings of the 7th European Wave and Tidal Energy Conference.

De Backer, G., Vantorre, M., De Beule, K., Beels, C., De Rouck, J., 2009. Experimental investigation of the validity of linear theory to assess the behaviour of a heaving point absorber at the belgian continental shelf. ASME.

FLOW-3D, 2009. User manual. Flow Science Inc.

Gilloteaux, J., Ducrozet, G., Babarit, A., Clement, A., 2007. Non-linear model to simulate large amplitude motions: application to wave energy conversion. Pr. of 22nd IWWFB.

Hu, Z., Causon, D., Mingham, C., Qian, L., 2009. Numerical wave tank study of a wave energy converter in heave. In: Proceedlings 19th ISOPE conference, Osaka, Japan. Vol. 1.

Li, Y., Yu, Y.-H., 2012. A synthesis of numerical methods for modeling wave energy converter-point absorbers. Renewable and Sustainable Energy Reviews 16 (6), 4352 – 4364.

Rahmati, M., Aggidis, G., Chaplin, R., 2008a. Investigating pitching-surge power-absorber wave energy converters. ASME POWER.

Rahmati, M., Aggidis, G. A., Chaplin, R., McCabe, A. P., 2008b. Test on a novel pitching-surge wave energy converter. In: Proceedings of World Renewable Energy Conference, WREC 2008.

Thilleul, O., Baudry, V., Guilcher, P., Scolan, Y., Jacquin, E., Babarit, A., Locuratolo, P., Larivain&8, A., 2011. Complementary use of a linear potential code, a rans and a sph solver for the optimisation of a wave energy converter. 9th European Wave and Tidal Energy Conference EWTEC.

Thomas, G., 2008. The theory behind the conversion of ocean wave energy: a review. Ocean wave energy, 41–91.